ATMOSPHERIC ENVIRONMENT: X 12 (2021) 100138

Contents lists available at ScienceDirect

Atmospheric Environment: X

journal homepage: www.journals.elsevier.com/atmospheric-environment-x

Triboelectrification-based particulate matter capture utilizing electrospun ethyl cellulose and PTFE spheres

Minhee Cho [a,1], Vishwanath Hiremath [b,1], Jeong Gil Seo [b,*]

[a] Department of Energy Science and Technology, Myongji University, Yongin, 17058, Republic of Korea
[b] Department of Chemical Engineering, Hanyang University, 222 Wangsimni-ro, Seongdong-gu, Seoul, 04763, Republic of Korea

ARTICLE INFO

Keywords:
Particulate matter capture
Triboelectrification
Ethylcellulose
Nanofibers
PTFE spheres

ABSTRACT

Air pollution associated with particulate matter (PM) has become one of the most serious environmental problems of the decade. Fibrous filters and electrostatic precipitators are usually employed to the indoor PM removal. In case of fibrous filter, if PM is smaller than the hole of filter, removal efficiency decreases considerably whereas, electrostatic precipitator has fatal drawback of producing unwanted O_3. In this study, triboelectric PM capture system was introduced by utilizing integrated mechanical filtration attributed to structural characteristic of electrospun ethylcellulose (EC) and the electrostatic filtration induced by the direct triboelectrification between electrospun EC and polytetrafluoroethylene (PTFE) spheres. The electrospun EC was reinforced by heating above glass transition temperature (T_g) to improve mechanical strength. Further, the triboelectrification between EC and PTFE achieved 100% PM removal efficiency and can eliminate the drawback of mechanical filtration without production of any hazardous substances. The improvement of PM removal efficiency by the triboelectrification were +6.68%, +6.89% and +5.47%, corresponding to PM_1, $PM_{2.5}$ and PM_{10} respectively. More importantly, it was observed that the triboelectric contribution was much higher for small PM which benefits overall system.

1. Introduction

Air contamination due to industrialization and urbanization has largely affecting the environment and human health (Kim et al., 2013; Brauer et al., 2012; Kinney, 2008). Among the major air pollutants, PM has attracted much attention because of its catastrophic effect on human health (WHO, 2013). Exposure to PM has led not only to respiratory and cardiovascular diseases but also to lung cancer since it can penetrate the respiratory system (Kim et al., 2015; Atkinson et al., 2010; Valavanidis et al., 2008; Brook et al., 2004, 2010; Guaita et al., 2011; Halonen et al., 2009)–(Kim et al., 2015; Atkinson et al., 2010; Valavanidis et al., 2008; Brook et al., 2004, 2010; Guaita et al., 2011; Halonen et al., 2009). PM which is a mixture of solid and liquid particles suspending in the air can be categorized mainly in to three classes based on the particle size, i) coarse particles (PM_{10}) with an aerodynamic diameter less than 10 μm, ii) fine particles ($PM_{2.5}$) with an aerodynamic diameter less than 2.5 μm and iii) ultrafine particles ($PM_{0.1}$, UFPs, a particle among $PM_{2.5}$) with an aerodynamic diameter less than 0.1 μm. Moreover, based on the source, PMs are further classified in to two subclasses i.e., primary PMs and secondary PMs which are emitted directly into the air and formed in the atmosphere by the photochemical reaction between gaseous precursors such as NO_x, SO_x, NH_3 and VOCs respectively (Trasande and Thurston, 2005; Juda-Rezler et al., 2011).

Considering these adverse effects on human health, PM removal systems are recommended which largely utilized to promote indoor air quality mainly working based on filtration methods (Cui et al., 2021; Lee et al., 2020). There are two typical filtration technologies in the indoor PM removal which are, fibrous filter such as HEPA filter (High efficiency particulate air filter) and electrospun nanofiber. The PM is removed via mechanical filtration induced by diffusion of PM and inertial impaction and interception between fibrous structure and PM particles (Sen Wang and Otani, 2013; Xiao et al., 2018). Although these technologies have been widely accepted and commercially established, numerous drawbacks have been listed. Fibrous filter has high efficiency to remove the PM particles with particle size larger than the holes because of the multilayer stacking. However, for UFPs which are much smaller than the holes of multilayer filter, its removal efficiency decrease considerably (Gu et al., 2017, 2018). In case of electrostatic precipitation, the PM

* Corresponding author.
E-mail address: jgseo@hanyang.ac.kr (J.G. Seo).
[1] These authors contributed equally.

https://doi.org/10.1016/j.aeaoa.2021.100138
Received 2 August 2021; Received in revised form 5 October 2021; Accepted 24 October 2021
Available online 27 October 2021

removal occurs through electrostatic filtration generated by corona discharge (Mizuno, 2000). It has advantages of low pressure drop and high collection efficiency compared to fibrous counterparts (Poppendieck et al., 2014). However, electrostatic precipitation has fatal drawback which inevitably generates ozone (O_3) through ionization of air that cause harmful effects on human health such as cancer (Chen and Davidson, 2003; Bo et al., 2010).

In recent times, electrospun polymer nanofibers linked with triboelectric nanogenerator (TENG) were introduced for PM capture to effectively resolve the problems associated with mechanical filtration technologies (Gu et al., 2017, 2018; Feng et al., 2017). Triboelectrification is a phenomenon in which material surface gets electrically charged as a result of contact, collision or friction with another material (Balestrin et al., 2014; Lacks and Mohan Sankaran, 2011). Also, these nanogenerators have attracted much attention due to their ability to generate electricity by utilizing wind, water, or external impact. Thus, harvesting an external source of energy to run self-powered devices has shaped new dimensions to boost sustainable development of environment applications. Recently, for PM removal applications, C. B. Han et al., reported self-powered triboelectric filter utilizing PTFE pellets and aluminum electrode induced by natural vibration of the tail pipe for PM removal from the automobile exhaust (Han et al., 2015). Also, H. J. Yoo at al., reported 3D-printed dust filter utilizing direct triboelectrification between acrylonitrile butadiene styrene (ABS) and PTFE powders (Yoon et al., 2019). Furthermore, promising applications have been reported for PM removal in air filters such as face masks (Bai et al., 2018; Liu et al., 2018).

Taking the que, in this study, we introduce PM capture system integrated with direct triboelectrification mechanical filtration. PM conditions have been mimicked such as indoor concentrations and the PM removal system has been developed to adopt to such conditions. The current device aims to promote indoor air quality via PM capture. Principally, ethylcellulose (EC) and polytetrafluoroethylene (PTFE) were selected for the triboelctric PM capture system based on the triboelectric series (Wang, 2013; Diaz and Felix-Navarro, 2004). EC is on the top of the triboelectric series which means it has highest potential to be positively charged. Whereas PTFE is on the bottom of the triboelectric series and carry a greater potential to be negatively charged, thanks to its inherent electronegativity. Electrostatic gradient between electrospun EC nanofiber and PTFE was induced via mechanical spinning which anticipated to eliminate the drawback of mechanical filtration including decrease of removal efficiency for smaller particles ranging from nanoparticles to microparticles without producing any hazardous substances such as ozone (O_3) (Sen Wang, 2001).

2. Materials and methods

Electrospinning is a technically straightforward, useful, and effective method that generates ultrathin polymer fibers uninterruptedly. In this study, binary solvent containing tetrahydrofuran (THF, Daejung chemicals, Korea) and N,N-dimethylacetamide (DMA, Daejung chemicals, Korea) were employed in order to conduct electrospinning of EC (10 cP, Daejung chemicals, Korea) (Park et al., 2007; Wu et al., 2005). In brief, certain amount of EC was dissolved in the binary solvent and stirred overnight until a homogeneous solution was obtained. The homogeneous solution was then transferred into a polypropylene syringe with a 0.5 mm inner diameter metal needle tip. The flow rate of the homogeneous solution was controlled by the syringe pump (EP100, NanoNC). The applied voltage was generated by power supply (HV power supply, HV30, NanoNC). Nanofibers were collected on an aluminum foil wrapped around drum-type collector (DC90, NanoNC) and on an aluminum mesh (size: 197 mm (W) x 197 mm (L), hole: 2.3 mm (W) x 3.2 mm (L), thickness: 0.4 mm). When the electrospinning was conducted on the aluminum mesh, the needle tip position was changed toward each edge of aluminum mesh to achieve the uniform thickness of nanofiber. Similarly, as a control group, a 10 wt% of polyacrylonitrile (PAN, average M_w 150,000, Sigma-Aldrich) solution was prepared by using dimethylformamide (DMF, Daejung chemicals, Korea) as a solvent and stirred overnight and electrospinning was carried using the similar method described above.

Morphologies of each electrospun nanofiber were investigated by using field emission scanning electron microscope (FE-SEM, SU-70, Hitachi) and elemental compositions of nanofiber were characterized by using energy dispersive X-ray spectroscopy (EDS, Energy X-MaxN, Horiba). The thermal behavior of electrospun EC was investigated by using thermo-gravimetric analyzer (TGA, TGA N-1000, SCINCO). TGA experiment was carried out by heating the sample from 25 °C to 700 °C at a ramping rate 10 °C/min under inert nitrogen (N_2) atmosphere. The glass transition temperature (Tg) of the electrospun EC was investigated by differential scanning calorimetry (DSC, DSC 3, METTLER TOLEDO). DSC analysis was conducted for 2 cycles of heating and cooling between 20 °C to 200 °C at rate of 10 °C/min under inert N_2 atmosphere at N_2 flow rate of 50 ml/min. The surface functional groups were analyzed by using fourier transform infrared spectroscopic method (FT-IR, Cary 630 FTIR, Agilent) using attenuated total reflectance (ATR) assembly.

PM removal tests were carried out in simulated indoor environment generated in an acrylic box (W:800 mm, D: 550 mm, H: 500 mm, thickness: 10 mm). The PM capture occurs in triboelectric layer (TL) built by using hollow acrylic frames (197 mm (W) x 197 mm (L) x 8 mm (H), thickness: 10 mm) which contains nanofiber concealed aluminum mesh at the bottom with highly dispersed PTFE spheres (D = 3.18 mm, GoodFellow, England) and then the top of the acrylic frame was covered by another aluminum mesh and fixed by using an aluminum tape. The TL was made such that sufficient gap exist between the two layers and PTFE spheres could easily spin. The TL was then placed in the triboelectric PM capture system (220 mm (W) x 220 mm (L) x 170 mm (H), thickness: 10 mm). In brief, the triboelectric PM capture system comprised of TL and a fan which allows the circulation of PM/air in and out of frame.

Further, the PM particles were generated by burning incense sticks inside the acrylic box to create a simulated indoor environment. The burning incense contains PM above 45 mg g^{-1} burned and It is identified that incense sticks produces more PM particles than cigarettes and also generates gaseous products such as CO, CO_2, NO_2 and SO_2 and organic compounds such as benzene, toluene, xylene, aldehydes and polycyclic aromatic hydrocarbons (Lin et al., 2008). The experiments are further explained in detail in the supporting information.

3. Results and discussion

Scheme 1(a) illustrates the schematic presentation of synthesis of electrospun EC on aluminum mesh. In general, morphology of electrospun nanofiber is highly influenced by process parameters such as, solution flow rate, applied voltage, needle tip-collector distance and solution parameters such as solution concentration and solvent ratio (Subbiah et al., 2005; Li and Xia, 2004; Deitzel et al., 2001)–(Subbiah et al., 2005; Li and Xia, 2004; Deitzel et al., 2001). Prior to applying electrospun nanofiber to filtration system, process parameters were optimized to avoid the formation of beads which primarily results from the agglomeration. If nanofiber contains beads in the fibrous structure, filtration capability decreases considerably due to the reduction of surface area. Subsequently, nanofiber loses mechanical properties. In present study, various parameters were assessed to find an optimal morphology of electrospun EC using drum type collector. At first, in order to find the best EC concentration, a series of EC concentrations including 13 wt%, 15 wt%, 17 wt% and 20 wt% were dissolved in a mixed solvent containing THF and DMA with volume ratio of THF:DMA = 2:8.

FE-SEM images revealed that nanofiber gradually appeared, and beads decreased with increase of EC concentration from 13 wt% to 20 wt % (figure. S1(a)(i-iv)). Initially, with EC concentration of 13 wt%, only beads were formed. Whereas, increasing concentration results in the

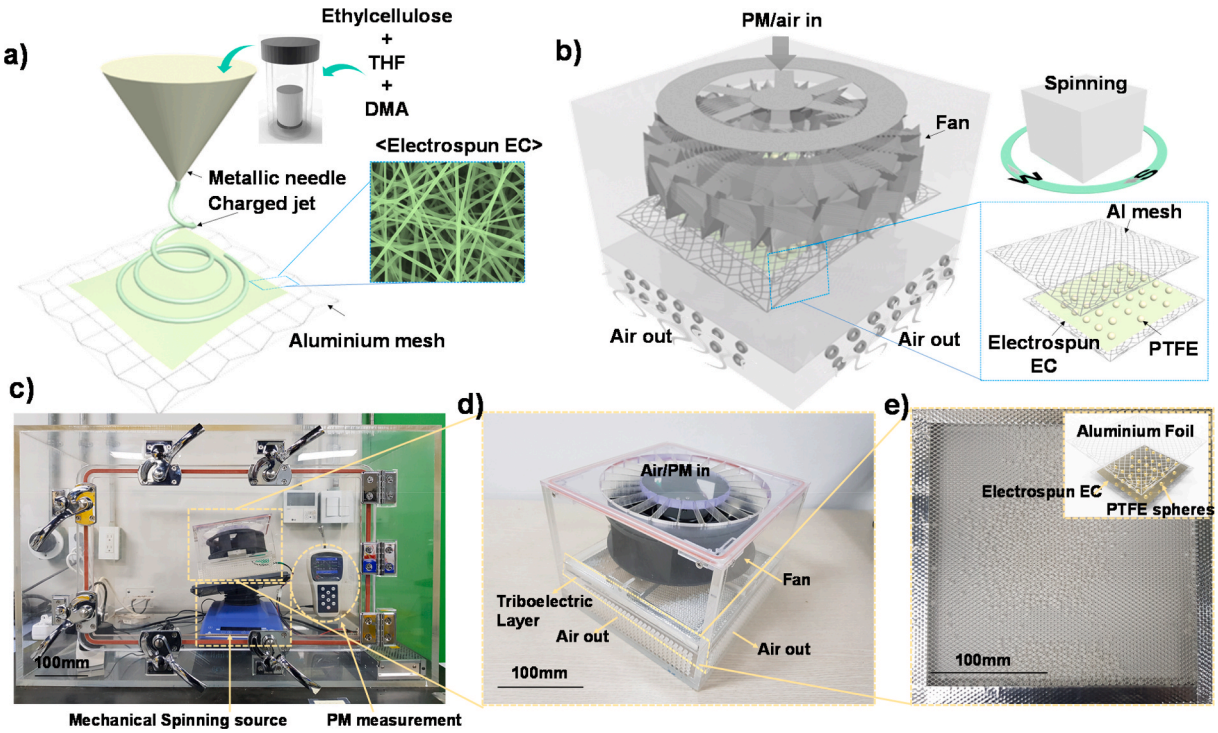

Scheme 1. Conceptual presentation of a) fabrication of electrospun EC over aluminum mesh using electrospinning method, b-e) lab-made triboelectric-based PM-removal system.

formation of fibrous structure. FE-SEM suggest that EC concentration of 20 wt% was optimal and could be adopted for further studies. Subsequently, solvent THF and DMA weight ratios were changed from THF: DMA = 2:8, 4:6 & 5:5 using 20 wt% EC. The FE-SEM (figure. S1(b)(i-iii)) images shows that at THF:DMA volume ratio of 5:5 shape better morphology than the other counterparts. Tuning the EC and solvent ratio, the formation of EC nanofiber was evidenced via sequence of morphological changes including beads to beads-fiber interconnections creating necklace-like morphology and at an optimized condition, the beads disappear and results in the formation of well interconnected nanofiber structures. A similar trend was obtained for change in the applied voltage (figure. S1(c)(i-v)) which suggest that 16 kV is an optimum voltage to fabricate well interconnected nanofibers with no beads. These optimization phases reveal that, EC concentration, solvent ratio and applied voltage influence the morphology of nanofibers mainly controlling the formation of beads. Consequently, the optimal solution concentration of EC was fixed to 20 wt% dissolved in the mixed solvent containing THF and DMA with the volume ratio of THF:DMA 5:5 and the optimal applied voltage was 16 kV.

With the optimized conditions, the collector was changed to aluminum mesh and the electrospinning was carried out. Unfortunately, we have witnessed different morphologies collected on aluminum mesh compared to drum-type collector. In the same conditions as that of tip-collector distance and solution flow rate which were the optimized conditions for drum collector, alumina mesh collector has shown formation of larger fiber with bisected morphology. We assume that this might be due to the accumulation of EC on the vertically aligned mesh-type collector. Hence, tip-collector distance as a function of flow rate was studied to avoid the formation of larger fibers with bisected morphology and to achieve optimal morphology. As assumed, FE-SEM images collected exposed that tip-collector distance indeed influenced the morphology (Figure. S2 (a-c)). Among the selected tip-collector distances (10 cm, 15 cm and 20 cm), 20 cm proved to be advantageous which produce finely interconnected nanofibers with no beads or bisections. Consequently, when aluminum mesh was used as collector, the optimized solution condition including EC concentration of 20 wt% dissolved in the mixed solvent with volume ratio THF:DMA = 5:5 was prepared as solution mixture. The optimized operational conditions involve tip-collector distance of 20 cm, applied voltage of 16 kV and solution flow rate of 19 μL/min. Subsequently, the well aligned EC nanofiber was achieved by applying these optimized parameters.

The as prepared nanofiber concealed aluminum mesh was utilized for the construction of PM-removal system. Scheme 1(b-e) shows the conceptual presentation and fabrication of triboelectric-based PM-capture system. The triboelectric PM-capture system mainly consists of fan and the TL. The TL was assembled using bare aluminum mesh on the top, electrospun EC concealed aluminum mesh on the bottom and in between PTFE spheres were dispersed as seen from Scheme 1(c-e). The dispersed PTFE spheres are only in contact with the bottom electrospun EC concealed aluminum mesh and expected to move freely to generate the triboelectrification.

To investigate the state of TL after mechanical agitation, few cycles of spinning were carried out and the state of TL was examined. Unluckily, the as concealed EC over alumina mesh was deformed due to the mechanical movement of PTFE spheres on its surface (Fig. 1(a)). This indicated that though EC fibers are well fabricated over aluminum mesh, they are mechanically fragile and undergoes easy deformation once the external forces are exerted.

The as prepared electrospun EC had a weak mechanical property such as fluffiness so it was easily scattered like a cotton candy by other external impacts such as wind and contact with other materials. Thus, when TL with as electrospun EC was fabricated, PTFE spheres and nanofiber became entangled together. Also, it shows complete deformation of EC which may result in the unsuccessful fabrication of the overall PM capture system. Because of this phenomenon, mechanical movement generating the triboelectrification was rapidly decreased. So, the modification of electrospun EC was essential to enable triboelectrification. It was found that the mechanical properties of electrospun nabofibers can be improved without any destruction of its nanofibrous morphology by heat treatment at a temperature above its glass transition temperature (T_g) (Zhang et al., 2012; Ma et al., 2005; Es-Saheb and Elzatahry, 2014). The glass transition is one of

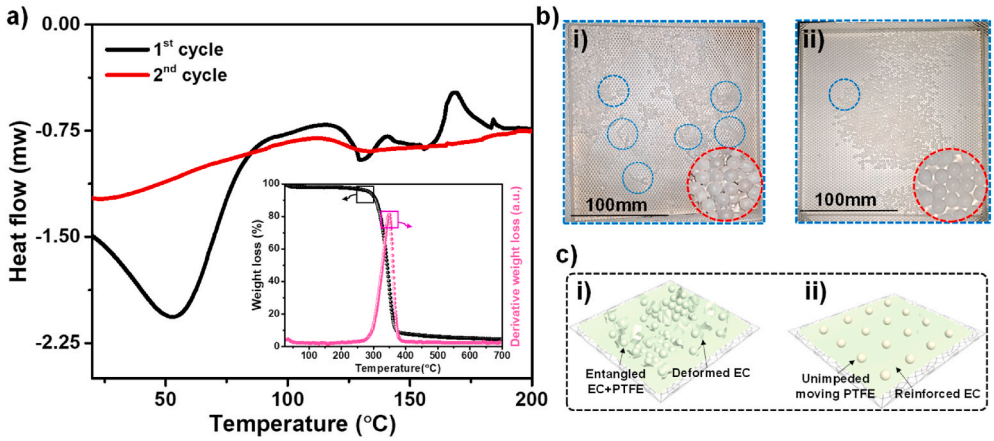

Fig. 1. a) DSC-curve of electrospun EC during first and second heating process and thermogram for as spun EC nanofiber (inset), b)(i-ii) the real time photographs and c)(i-ii) the schematic presentation of TL before and after the heating above glass transition temperature respectively.

characteristics of the polymers which have certain degree of amorphous portions. Ethylcellulose has a semi-crystalline structure that has crystalline domains within an amorphous content (Davidovich-Pinhas et al., 2014).

Thermal behavior of electrospun ethyl cellulose was investigated to determine the heat treatment temperature. Fig. 1(a) (inset) shows the TG-DTA result of electrospun EC carried out in the temperature window of 25–700 °C at a heating rate of 10 °C/min. The thermogram displays that EC started to decompose above around 200 °C. Therefore, the heat treatment must be carried out below 200 °C. Further, to figure out the exact required temperature, DSC analysis was carried out (Fig. 1(a)). DSC results showed that T_g of electrospun ethylcellulose was observed at ~128 °C during first heating process and ~125 °C during second heating process. Based on these observations, electrospun ethylcellulose was heated at 130 °C which is above T_g for 1 h in convection oven. During the heat treatment process, the polymer chains of electrospun EC were rearranged and when cooled down below T_g, it became hard gaining mechanical strength. As expected, the heat-treated nanofiber retained its morphology without undergoing any change (Fig. 1 (b)(i-ii)). By resolving this issue, PTFE spheres and heat treated electrospun EC are

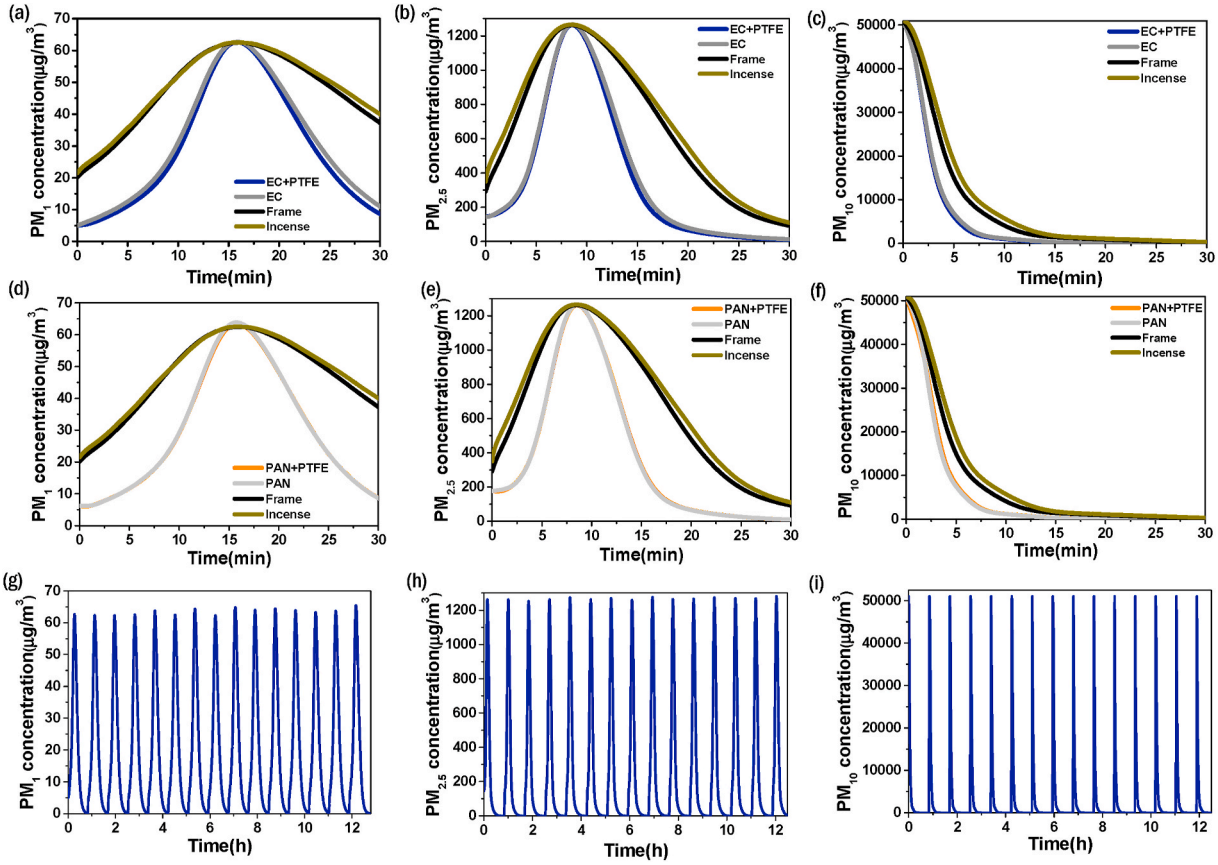

Fig. 2. PM capture evaluation of TL with EC + PTFE and TL with EC. (a) PM_1 concentration change. (b) $PM_{2.5}$ concentration change. (c) PM_{10} concentration change, PM capture evaluation of TL with PAN + PTFE and TL with PAN. (d) PM_1 concentration change. (e) $PM_{2.5}$ concentration change. (f) PM_{10} concentration change, 15 cyclic tests of the TL with EC + PTFE. (g) PM_1 concentration change. (h) $PM_{2.5}$ concentration change. (i) PM_{10} concentration change.

again imbedded into TL filter system which shows no entanglement and allows unimpeded movement of PTFE spheres and successfully promoting triboelectrification.

After successful establishment of TL and the developing a PM capture system, the PM capture studies were conducted for TL with EC and EC + PTFE. In comparison, TL with PAN and PAN + PTFE were also evaluated as a control. PAN is located in lower position than EC in the triboelectric series which indicates that PAN has a much lesser tendency to be positively charged than EC when it contacts the PTFE spheres (Wang, 2013; Diaz and Felix-Navarro, 2004). Also, EC is on the top of the triboelectric series than nylon which is one of the well-known materials to become positively charged. Fig. 2 shows the results of PM removal tests including frame, EC, and EC + PTFE. Frame means the PM capture system without TL. This helps to differentiate the contribution of triboelectric effect, mechanical filtration, and the influence of the frame of the system on PM capture. The maximum mass concentration observed for each PM were 62.5, 1,270, 50,988 μg/m^3 for $PM_{1.0}$, $PM_{2.5}$, and PM_{10}, respectively. In all the cases TL comprised of EC + PTFE showed the better capability to remove the PMs than the TL with EC (Fig. 2(a–c)). Fig. 2(d–f) shows the results of PM removal tests of TL comprising PAN + PTFE and the TL with PAN. Clearly, the triboelectrification effect was almost absent in the TL with PAN + PTFE. Further, cyclic tests were carried out to check reproducbity and stability of the system. As seen from Fig. 2(g–i)), EC + PTFE shows excellent stability.

Fig. 3 shows the quantification of PM capture efficiency differentiated by using triboelectric effect, mechanical filtration, and removal by frame for TL with EC + PTFE and TL with.

PAN + PTFE. As observed from Fig. 3(a), maximum increase of PM_1 removal efficiency by the triboelectrification was +6.68% and Fig. 3(b) shows that the maximum increase of $PM_{2.5}$ removal efficiency by the triboelectrification was +6.89%. Some of PM_1 and $PM_{2.5}$ can be captured by mechanical filtration such as inertial impaction, interception and brownian diffusion but they could pass the electrospun EC if the pores of nanofiber are bigger than PM particle. However, it is believed that in presence of triboelectrification induced between EC and PTFE, PM_1 and $PM_{2.5}$ can be more captured on the EC nanofiber or PTFE surface by the electrostatic attractions. This clearly demonstrate that triboelectric effect has played a key role in capture of smaller $PM_{1.0}$ and $PM_{2.5}$ which otherwise could pass through the pores of EC. In Fig. 3(c), the maximum increase of PM_{10} removal efficiency by the triboelectrification was +5.47%. The particle size of PM_{10} is bigger than PM_1 and $PM_{2.5}$ so PM_{10} was relatively easy to be captured than PM_1 and $PM_{2.5}$ by the mechanical filtration. However, its removal efficiency can further be enhanced by triboelectrification. On the other hand, in the case of the control group, the triboelectrification effect in the PM capture was almost negligible amounts (Fig. 3(d–f)). Based on these observations, we have plotted correlation diagrams to clearly differentiate the various factors controlling the PM removal efficiency. Fig. 3(g–i) shows the comparison of removal efficiency enhancement between the TL with EC + PTFE and the TL with PAN + PTFE. From the correlation diagrams it is evident that, the TL with PAN shows better PM removal efficiency than the TL with PAN + PTFE. In other words, there was no apparent effect of triboelectrification in the control group. On the other

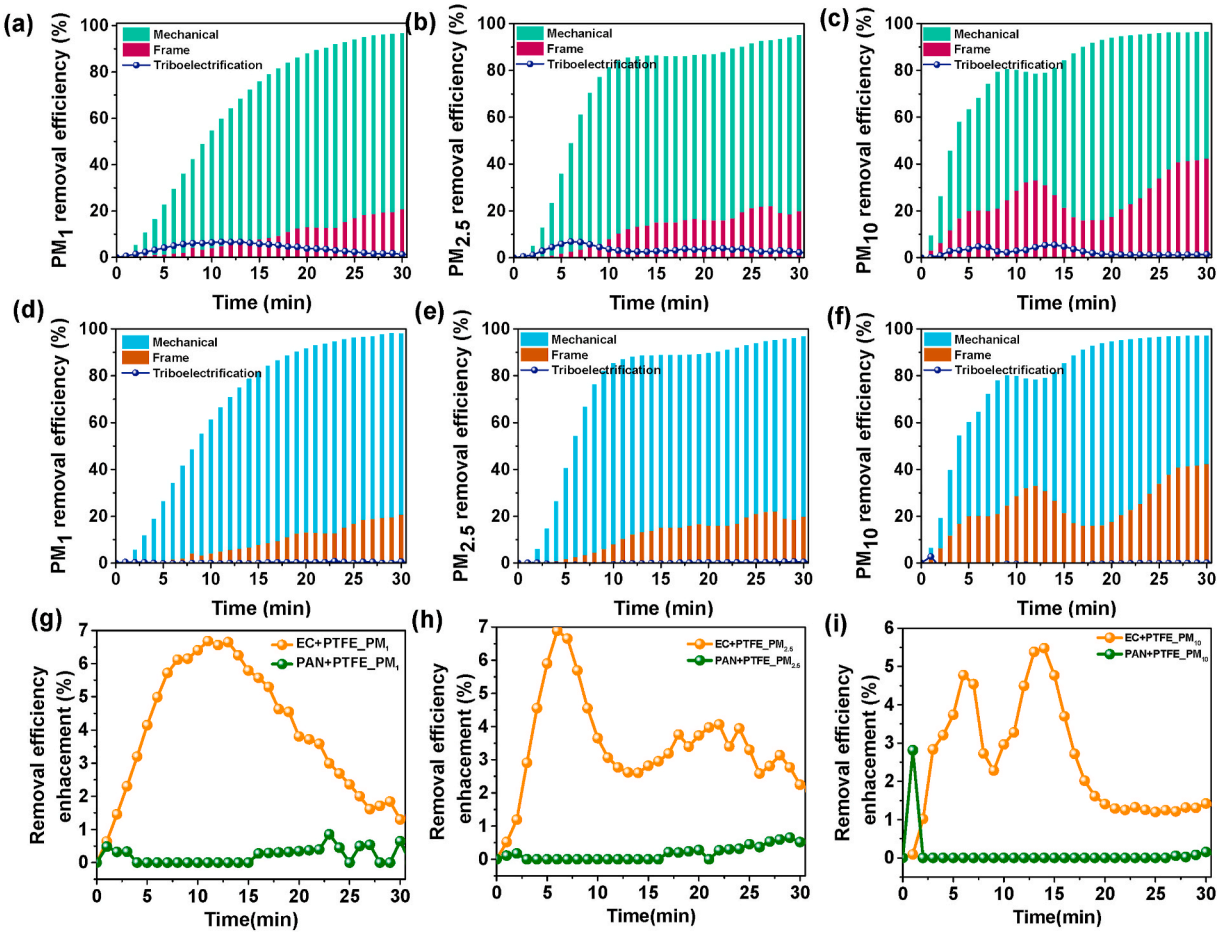

Fig. 3. Removal efficiency of (a) PM_1, (b) $PM_{2.5}$ and (c) PM_{10} of the TL with EC + PTFE and the removal efficiency of (d) PM_1, (e) $PM_{2.5}$ and (f) PM_{10} of the TL with PAN + PTFE. (The time value of x-axis is started from each peak of the PM mass concentration in Figure S4-S5), and removal efficiency enhancement by the triboelectrification of (g) PM_1, (h) $PM_{2.5}$ and (i) PM_{10} of EC + PTFE and PAN + PTFE.

hand, the triboelectrification between EC and PTFE showed the obvious improvement of the removal efficiency in the PM capture. Moreover, it showed that smaller the particle size of PM, higher the triboelectrification influences and thus enhances the PM capture capability.

Despite their capability to efficiently capture PM, cyclic stability plays major role in establishing commercial platforms. In order to evaluate the cyclic stability, EC + PTFE TL was tested for 15 cycles. Figure S5 shows the 15 cyclic tests of the TL with EC + PTFE. During 15 cyclic tests, EC + PTFE has maintained 100% removal efficiency and 100% retainment in its cyclic stability exhibiting advantageous feature of integrated PM removal system. The behaviors of PMs in the capture process by the electrospun nanofiber are quite different because they have different chemical compositions, morphologies and mechanical properties (Hinds, 1998). In the case of rigid inorganic PMs, they are attached to the surface of nanofiber by interception and inertial impaction. However, in the case of soft PMs containing carbon compounds and water produced from combustion exhaust, they strongly wrap the surface of nanofiber and deform their shape during the capture process instead of attaching like the inorganic PMs (Liu et al., 2015, 2019). As a fact, the TL exhibits the color transformation from the white to the brownish yellow (figure S3).

Furthermore, to elucidate the mechanism of PM capture by electrospun EC, the FE-SEM analysis was carried out for samples after certain interval of time. Fig. 3 shows the PM capture process of the electrospun EC and the sequence morphological change after PM capture. Before the PM capture, the morphology of the electrospun EC showed the regular nanofiber structure and smooth surface (Fig. 4(a)).

At the initial step of the PM capture, PMs were captured to the nanofiber by the mechanical filtration and the electrostatic attraction attributed to the triboelectrification (Fig. 3(b)). The captured PMs were then wrapped around the nanofiber and combined along the nanofiber and made the bulged morphology (Fig. 4(c–d)). When more smoke PMs pass through the TL, PMs were attached on the nanofiber or the existing PM and then made the bigger bulged shape. After considerable PM capture, the captured PMs covered the nanofiber, so it made the nanofiber thicker as schematically shown in Fig. 4. At the same time as observed from the corresponding diameter distribution of the nanofibers, thicker nanofiber diameters could be observed. These observations reveal that the interaction between EC and the PM are promoted via triboelectrification which transforms the morphology. Contrarily, PTFE spheres were also evaluated using FE-SEM after a certain interval of time as that of EC. The surface of PTFE sphere was smooth and clean before the PM capture (figure S4(a)). The PTFE surface got negatively charged by the triboelectrification, so it had electrostatic attraction capturing the PM (figure S4(b)). Soft PMs were attracted and attached on the PTFE surface and then its shape deformed to the reticulate morphology (figure S4(c). Based on these observations, mechanism of PM removal in absence and presence of triboelctric effect has been drawn as shown in Scheme 2(a&b). Scheme 2(a) depicts the mechanism of PM removal via mechanical filtration without the triboelectrification. The filtration layer comprised of only electorpsun EC has the mechanical filtration attributed to the structural characteristics of electrospun nanofiber such as interception, inertial impaction, and diffusion. But if the hole of the electrospun nanofiber is bigger than PM, some of small PM can penetrate which is an obvious reason for lower filtration efficiency. Scheme 2(b) illustrates the PM capture mechanism integrated with the triboelectrification. The electrospun EC and PTFE spheres are contacted or collided each other under mechanical movement. As a result, PTFE receives the electron from EC because of its high electronegativity and subsequently PTFE become negatively charged and EC become positively charged. At this state of the TL, PMs can be more effectively captured by both mechanical filtrations attributed to the

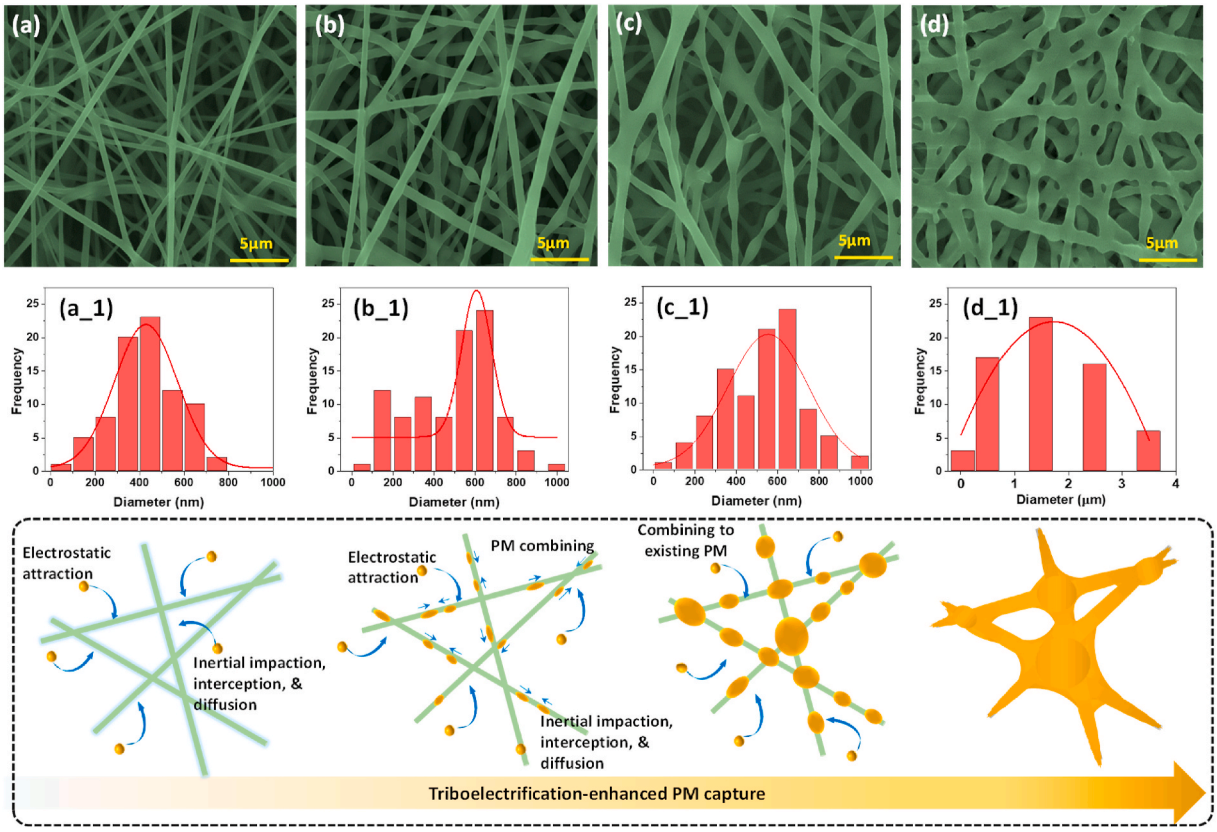

Fig. 4. The PM capture process of the electrospun EC and the sequential morphological changes after PM capture. (a) electrospun EC before PM capture, (b–d) ElectrospunEC after PM capture with bulged morphology, (c) Electrospun EC after PM capture with bigger bulged morphology, (d) Electropsun EC after PM capture with covered morphology, and their corresponding diameter distribution of nanofibers (a_1-d_1).

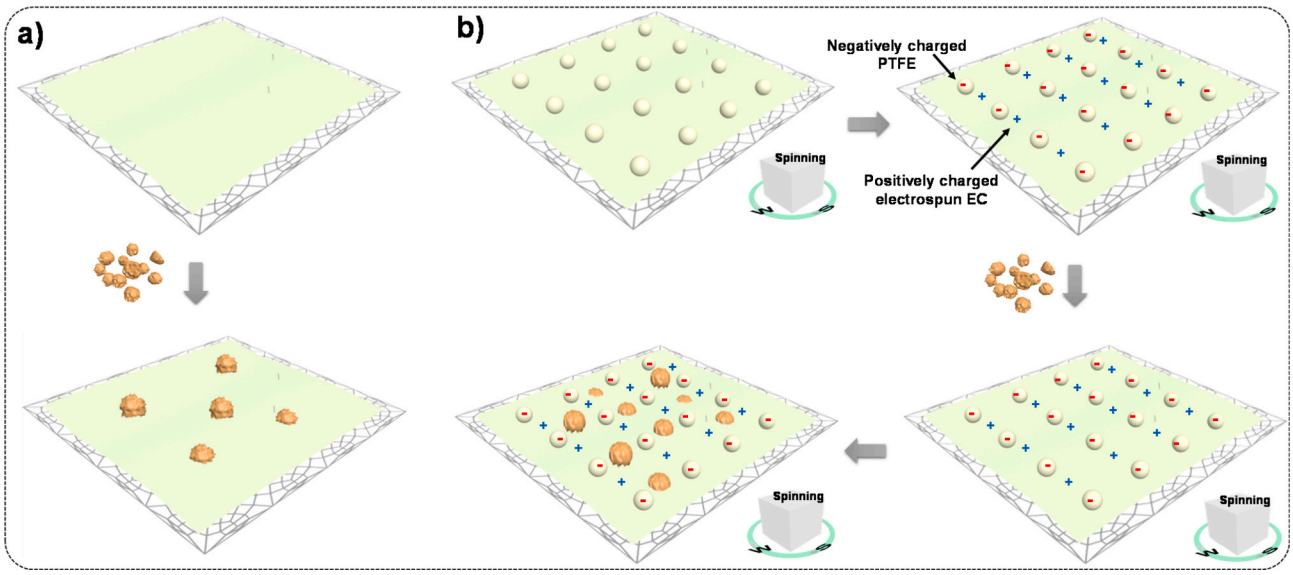

Scheme 2. PM capture mechanism of (a) TL comprised of electrospun EC and (b) TL comprised of electrospun EC and PTFE spheres.

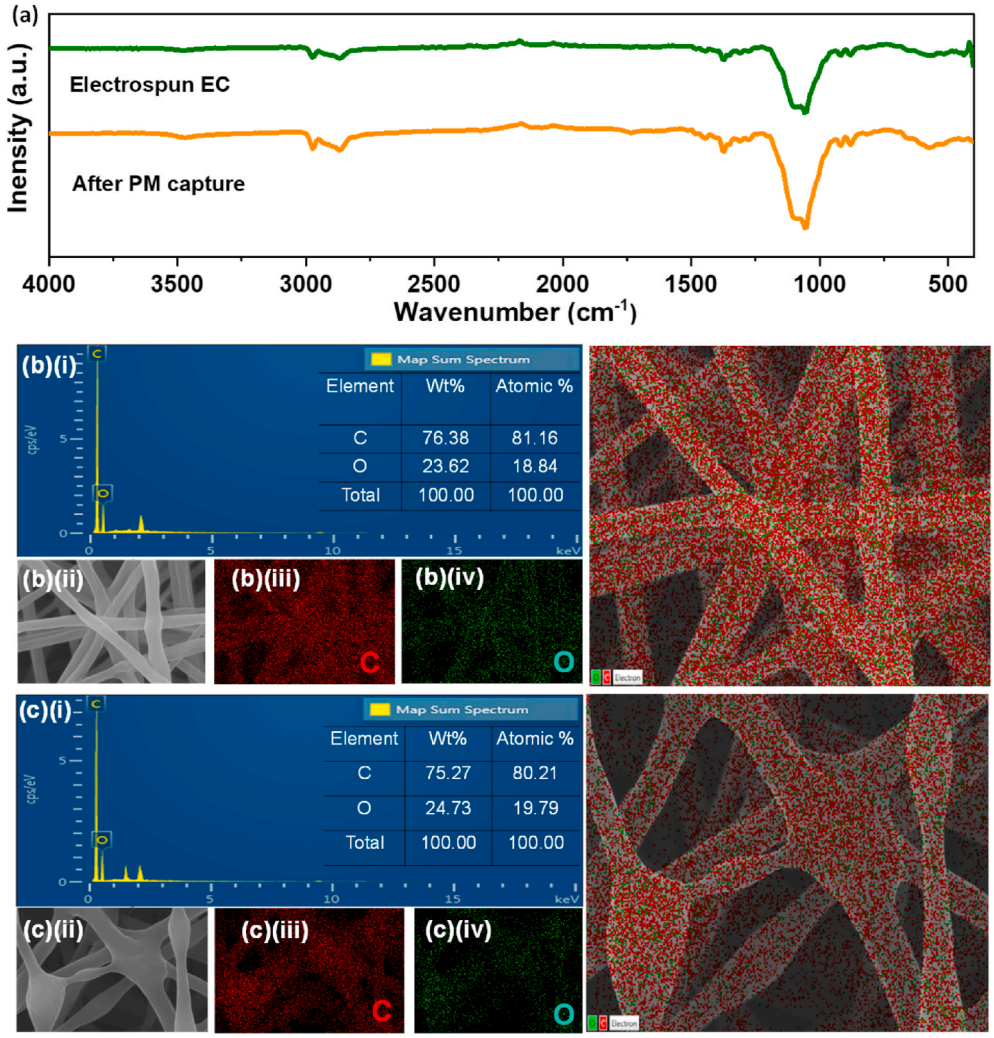

Fig. 5. (a) FT-IR spectra of electrospun EC before and after the PM capture. EDS results of (b) electrospun EC before the PM capture, and (c) electrospun EC after the PM capture.

structural characteristic of the electrospun nanofiber and electrostatic filtration induced by triboelectrification.

Furthermore, FT-IR was conducted to confirm the change of the surface functional group before and after the PM capture. In Fig. 5(a), the pristine electrospun EC showed several peaks at 3488.7, 1274.7, 1051.2 and 916.9 cm^{-1} which are attributed to O–H, C–O, C–O and C–O. Additionally, two peaks observed at 2870 and 2974.4 cm^{-1} are attributed to the symmetric and asymmetric stretching vibration of CH_2 group of EC. Conversely, the sample after the PM capture showed the increase in the intensity attributed to captured PM particles which is in line with the obtained EDS results. Specifically, the intensity of the peak located at 1736 cm^{-1} which is attributed to C═O was increased due to the captured PM. Consequently, the functional group which the captured PMs have are C–H, C–O and C═O. In order to analyze the composition of the captured PMs, EDS analysis was carried out for samples before and after PM capture.

The EDS result of the electrospun EC before and after PM capture showed a little change in the element compositions of C and O (Fig. 5 (b&c)). Since, the PM is also composed of C and O, no recognizable results were seen. Elemental mapping shows that in line with the morphological changes, the deformed structures constitute of C and O. However, the compositions of PAN nanofiber showed some changes (Figure S5). Oxygen element appeared on the PAN nanofiber after the PM capture (Figure S5(b)). From these results, the element compositions of the captured PMs could be discovered that they consist of C and O.

Taking advantage of physicochemical properties of EC and PTFE, we present simple wash with water to assess the reusability of the TL comprised of the electrospun EC and PTFE spheres. Inherently, EC is hydrophobic in nature so the captured PMs on the EC nanofiber can be removed from the surface by washing with water. In addition, PTFE is also hydrophobic polymer so the captured PMs on the surface can also be removed by water. To confirm the structural integrity of the electrospun EC, FT-IR analysis was carried out after water washing. As shown in figure 5a, the result express similar peaks with no major changes as that of the pristine electrospun EC which validate the structural integrity of EC nanofiber. Electrospun EC has shown increased intensity of peaks located at 2974.4, 2870, 1274.7, 1051.2 and 916.9 cm^{-1}, corresponding to C–H, C–H, C–O, C–O and C–O respectively, after PM capture. However, after water wash the intensity of these peaks has been decreased which confirms that the captured PMs were almost removed well. However, in line with SEM result, there was peak at 1736 cm^{-1} which is attributed to C═O which may be due to that residue present on the stacked layers of the electrospun EC. Even though there was a little residual captured PM, Fig. 5(b) shows that the PMs were almost all removed without any change of the nanofiber morphology. Furthermore, Fig. 5(c) confirms the absence of reticulate structures on the PTFE which indicates the complete removal of surface attached PM particles. However, there were some holes and cracks on the surface because of the collision during the triboelectrification. After washing experiments, the TL was again assembled by using the washed EC and PTFE spheres to assess the PM capture capability (figure S6 (a-c)). The TL comprised of EC + PTFE showed the better removal efficiency than the TL with EC over all PMs, which validate the presence of triboelectrification effect. Fig. 6(f–h) shows the quantification of the triboelectrification effect of the TL with EC + PTFE in the PM capture after washing. The quantification revealed that maximum increase of PM removal efficiency by triboelectrification was +7.6%, +8.67%, and +3.97% for $PM_{1.0}$, $PM_{2.5}$, and PM_{10} respectively. Furthermore, TL with EC + PTFE after washing maintained good removal capability for 15 cyclic tests (figure S7).

Furthermore, the pressure drop experiments were conducted using electrospun EC filter under different wind velocities. Pressure drop experiments are indicative of energy input for the gas in/out of the filter which further determines the efficiency. Fig. 7(inset) shows the experimental setup and Fig. 6 shows the pressure drop as a function of wind velocity. The pressure drops of the electrospun EC were 65, 129, 230,329 and 382 Pa at the wind velocity of 0.1, 0.2, 0.3, 0.4 and 0.45 m/s respectively, which were <0.38% of atmospheric pressure. Though, with increase in the.

wind velocity, increase in the pressure drop was observed, the obtained values are smaller than other PAN-based air filters (Liu et al., 2015). The thermally reinforced EC shows stability over multiple cyclic tests after washing as well for pressure drop tests which shows likely benefits of present study. Nevertheless, the overall improved efficiency attributed to synergistic mechanical filtration and triboelectric effects

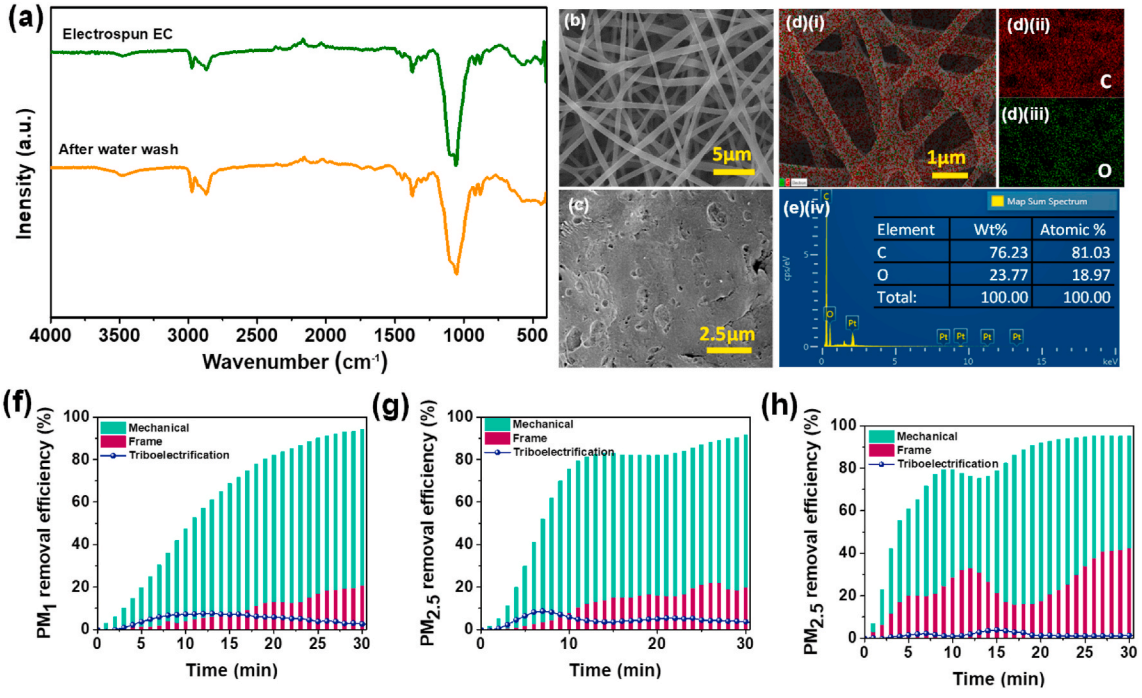

Fig. 6. a) FT-IR analysis of the electrospun EC after washing, FE-SEM images of (b) the electrospun EC and (c) the PTFE spheres after washing. EDS result of (d–e) the electrospun EC after washing, removal efficiency of (f) PM_1, (g) $PM_{2.5}$ and (h) PM_{10} of the TL with EC + PTFE after washing.

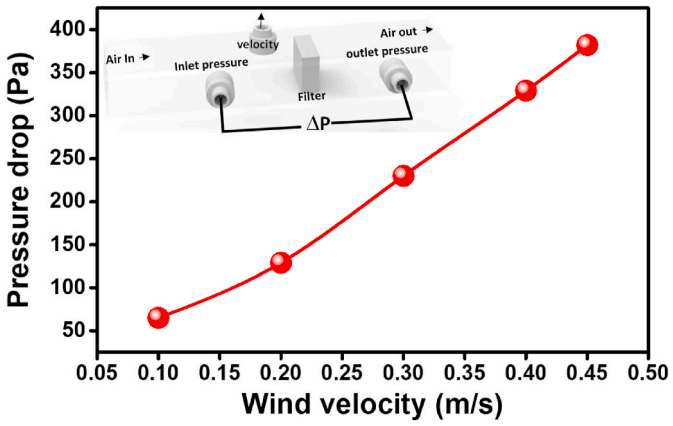

Fig. 7. The pressure drop as function of wind velocity using electrospun EC as filter (Inset shows the schematic presentation of experimental setup for the pressure drop analysis.).

using mechanical spinning. Triboelectric effect played key role in removal of smaller PM with improved efficiency and kinetics whereas, mechanical filtration could be able to filter larger PM. The order of triboelectric effect contribution to enhance the removal found to be $PM_{1.0} > PM_{2.5} > PM_{10}$.

4. Conclusions

In summary, we have successfully demonstrated the fabrication of PM-removal system to utilize triboelectrification to capture PM-particles simulating typical atmospheric conditions. The improved removal efficiency is attributed to synergetic impact between mechanical filtration credited to fibrous structure and triboelectrification fetched in by PTFE spheres and electrospun EC. We have clearly shown simplest measure to remove mechanical damage to electrospun EC and reinforced its mechanical strength via thermal treatment which shows excellent stability for improved cyclic efficiency. Further, the triboelectrification between EC and PTFE achieved 100% PM removal efficiency and can eliminate the drawback of mechanical filtration without production of any hazardous substances. More importantly, the PM-removal system shows better performance towards smaller PM ($PM_{1.0}$ and $PM_{2.5}$). The triboelectrification contribution were found to be +6.68%, +6.89% and +5.47%, corresponding to $PM_{1.0}$, $PM_{2.5}$ and PM_{10} respectively. Overall, the present system shows promising results and with further improvement in the PM-capture system, has greater potential for commercial platform to promote indoor or outdoor air quality by harvesting simple mechanical movement.

Authors statement

The author contributed solely to the intellectual discussion underlying this paper, literature exploration, writing, and editing, and accepts responsibility for the content and interpretation.

Declaration of competing interest

The authors declare that they have no known competing financial interests or personal relationships that could have appeared to influence the work reported in this paper.

Acknowledgment

This work was supported by the National Research Foundation of Korea (NRF) grant funded by the Korea government (MSIT) (No. 2019R1A2C1090304 and No. 2020R1C1C1010085). This work was also supported by the Graduate school of Post Plastic specialization of Korea Environmental Industry & Technology Institute grant funded by the Ministry of Environment, Republic of Korea.

Appendix A. Supplementary data

Supplementary data related to this article can be found at https://doi.org/10.1016/j.aeaoa.2021.100138.

References

Atkinson, R.W., Fuller, G.W., Anderson, H.R., Harrison, R.M., Armstrong, B., 2010. Urban ambient particle metrics and health: a time-series analysis. Epidemiology 21, 501–511. https://doi.org/10.1097/EDE.0b013e3181debc88.

Bai, Y., Han, C.B., He, C., Gu, G.Q., Nie, J.H., Shao, J.J., Xiao, T.X., Deng, C.R., Wang, Z. L., 2018. Washable multilayer triboelectric air filter for efficient particulate matter PM2.5 removal. Adv. Funct. Mater. 28, 1–8. https://doi.org/10.1002/adfm.201706680.

Balestrin, L.B.D.S., Del Duque, D., Da Silva, D.S., Galembecka, F., 2014. Triboelectricity in insulating polymers: evidence for a mechanochemical mechanism. Faraday Discuss 170, 369–383. https://doi.org/10.1039/c3fd00118k.

Bo, Z., Yu, K., Lu, G., Mao, S., Chen, J., Fan, F.G., 2010. Nanoscale discharge electrode for minimizing ozone emission from indoor corona devices. Environ. Sci. Technol. 44, 6337–6342. https://doi.org/10.1021/es903917f.

Brauer, M., Amann, M., Burnett, R.T., Cohen, A., Dentener, F., Ezzati, M., Henderson, S. B., Krzyzanowski, M., Martin, R.V., Van Dingenen, R., Van Donkelaar, A., Thurston, G.D., 2012. Exposure assessment for estimation of the global burden of disease attributable to outdoor air pollution. Environ. Sci. Technol. 46, 652–660. https://doi.org/10.1021/es2025752.

Brook, R.D., Franklin, B., Cascio, W., Hong, Y., Howard, G., Lipsett, M., Luepker, R., Mittleman, M., Samet, J., Smith, S.C., Tager, I., 2004. Air pollution and cardiovascular disease: a statement for healthcare professionals from the expert panel on population and prevention science of the American Heart Association. Circulation 109, 2655–2671. https://doi.org/10.1161/01.CIR.0000128587.30041.C8.

Brook, R.D., Rajagopalan, S., Pope, C.A., Brook, J.R., Bhatnagar, A., Diez-Roux, A.V., Holguin, F., Hong, Y., Luepker, R.V., Mittleman, M.A., Peters, A., Siscovick, D., Smith, S.C., Whitsel, L., Kaufman, J.D., 2010. Particulate matter air pollution and cardiovascular disease: an update to the scientific statement from the american heart association. Circulation 121, 2331–2378. https://doi.org/10.1161/CIR.0b013e3181dbece1.

Chen, J., Davidson, J.H., 2003. Ozone production in the negative DC corona: the dependence of discharge polarity. Plasma Chem. Plasma Process. 23, 501–518. https://doi.org/10.1023/A:1023235032455.

Cui, J., Lu, T., Li, F., Wang, Y., Lei, J., Ma, W., Zou, Y., Huang, C., 2021. Flexible and transparent composite nanofibre membrane that was fabricated via a "green" electrospinning method for efficient particulate matter 2.5 capture. J. Colloid Interface Sci. 582, 506–514. https://doi.org/10.1016/j.jcis.2020.08.075.

Davidovich-Pinhas, M., Barbut, S., Marangoni, A.G., 2014. Physical structure and thermal behavior of ethylcellulose. Cellulose 21, 3243–3255. https://doi.org/10.1007/s10570-014-0377-1.

Deitzel, J.M., Kleinmeyer, J., Harris, D., Beck Tan, N.C., 2001. The effect of processing variables on the morphology of electrospun. Polymer 42, 261–272.

Diaz, A.F., Felix-Navarro, R.M., 2004. A semi-quantitative tribo-electric series for polymeric materials: the influence of chemical structure and properties. J. Electrost. 62, 277–290. https://doi.org/10.1016/j.elstat.2004.05.005.

Es-Saheb, M., Elzatahry, A., 2014. Post-heat treatment and mechanical assessment of polyvinyl alcohol nanofiber sheet fabricated by electrospinning technique. Int. J. Polym. Sci. 2014 https://doi.org/10.1155/2014/605938.

Feng, Y., Ling, L., Nie, J., Han, K., Chen, X., Bian, Z., Li, H., Wang, Z.L., 2017. Self-powered electrostatic filter with enhanced photocatalytic degradation of formaldehyde based on built-in triboelectric nanogenerators. ACS Nano 11, 12411–12418. https://doi.org/10.1021/acsnano.7b06451.

Gu, G.Q., Han, C.B., Lu, C.X., He, C., Jiang, T., Gao, Z.L., Li, C.J., Wang, Z.L., 2017. Triboelectric nanogenerator enhanced nanofiber air filters for efficient particulate matter removal. ACS Nano 11, 6211–6217. https://doi.org/10.1021/acsnano.7b02321.

Gu, G.Q., Han, C.B., Tian, J.J., Jiang, T., He, C., Lu, C.X., Bai, Y., Nie, J.H., Li, Z., Wang, Z.L., 2018. Triboelectric nanogenerator enhanced multilayered antibacterial nanofiber air filters for efficient removal of ultrafine particulate matter. Nano Res 11, 4090–4101. https://doi.org/10.1007/s12274-018-1992-1.

Guaita, R., Pichiule, M., Mate, T., Linares, C., Diaz, J., 2011. Short-term impact of particulate matter (PM2.5) on respiratory mortality in Madrid. Int. J. Environ. Health Res. 21, 260–274. https://doi.org/10.1080/09603123.2010.544033.

Halonen, J.I., Lanki, T., Yli-Tuomi, T., Tiittanen, P., Kulmala, M., Pekkanen, J., 2009. Particulate air pollution and acute cardiorespiratory hospital admissions and mortality among the elderly. Epidemiology 20, 143–153. https://doi.org/10.1097/EDE.0b013e31818c7237.

Han, C.B., Jiang, T., Zhang, C., Li, X., Zhang, C., Cao, X., Wang, Z.L., 2015. Removal of particulate matter emissions from a vehicle using a self-powered triboelectric filter. ACS Nano 9, 12552–12561. https://doi.org/10.1021/acsnano.5b06327.

Hinds, W.C., 1998. Aerosol Technology: Properties, Behavior, and Measurement of Airborne Particles. Wiley.

Juda-Rezler, K., Reizer, M., Oudinet, J.P., 2011. Determination and analysis of PM10 source apportionment during episodes of air pollution in Central Eastern European urban areas: the case of wintertime 2006, Atmos. Environ. Times 45, 6557–6566. https://doi.org/10.1016/j.atmosenv.2011.08.020.

Kim, K.-H., Jahan, S.A., Kabir, E., 2013. A review on human health perspective of air pollution with respect to allergies and asthma. Environ. Int. 59, 41–52. https://doi.org/10.1016/j.envint.2013.05.007.

Kim, K.H., Kabir, E., Kabir, S., 2015. A review on the human health impact of airborne particulate matter. Environ. Int. 74, 136–143. https://doi.org/10.1016/j.envint.2014.10.005.

Kinney, P.L., 2008. Climate change, air quality, and human health. Am. J. Prev. Med. 35, 459–467. https://doi.org/10.1016/j.amepre.2008.08.025.

Lacks, D.J., Mohan Sankaran, R., 2011. Contact electrification of insulating materials. J. Phys. D Appl. Phys. 44 https://doi.org/10.1088/0022-3727/44/45/453001.

Lee, M., Ojha, G.P., Oh, H.J., Kim, T., Kim, H.Y., 2020. Copper//terbium dual metal organic frameworks incorporated side-by-side electrospun nanofibrous membrane: a novel tactics for an efficient adsorption of particulate matter and luminescence property. J. Colloid Interface Sci. 578, 155–163. https://doi.org/10.1016/j.jcis.2020.05.113.

Li, D., Xia, Y., 2004. Electrospinning of nanofibers: reinventing the wheel? Adv. Mater. 16, 1151–1170. https://doi.org/10.1002/adma.200400719.

Lin, T.C., Krishnaswamy, G., Chi, D.S., 2008. Incense smoke: clinical, structural and molecular effects on airway disease. Clin. Mol. Allergy 6, 1–9. https://doi.org/10.1186/1476-7961-6-3.

Liu, C., Hsu, P.C., Lee, H.W., Ye, M., Zheng, G., Liu, N., Li, W., Cui, Y., 2015. Transparent air filter for high-efficiency PM 2.5 capture. Nat. Commun. 6, 1–9. https://doi.org/10.1038/ncomms7205.

Liu, G., Nie, J., Han, C., Jiang, T., Yang, Z., Pang, Y., Xu, L., Guo, T., Bu, T., Zhang, C., Wang, Z.L., 2018. Self-powered electrostatic adsorption face mask based on a triboelectric nanogenerator. ACS Appl. Mater. Interfaces 10, 7126–7133. https://doi.org/10.1021/acsami.7b18732.

Liu, H., Huang, J., Mao, J., Chen, Z., Chen, G., Lai, Y., 2019. Transparent antibacterial nanofiber air filters with highly efficient moisture resistance for sustainable particulate matter capture. IScience 19, 214–223. https://doi.org/10.1016/j.isci.2019.07.020.

Ma, Z., Kotaki, M., Ramakrishna, S., 2005. Electrospun cellulose nanofiber as affinity membrane. J. Memb. Sci. 265, 115–123. https://doi.org/10.1016/j.memsci.2005.04.044.

Mizuno, A., 2000. Electrostatic precipitation. IEEE Trans. Dielectr. Electr. Insul. 7, 615–624. https://doi.org/10.1109/94.879357.

Park, J.Y., Han, S.W., Lee, I.H., 2007. Preparation of electrospun porous ethyl cellulose fiber by THF/DMAc binary solvent system. J. Ind. Eng. Chem. 13, 1002–1008.

Poppendieck, D.G., Rim, D., Persily, A.K., 2014. Ultrafine particle removal and ozone generation by in-duct electrostatic precipitators. Environ. Sci. Technol. 48, 2067–2074. https://doi.org/10.1021/es404884p.

Sen Wang, C., 2001. Electrostatic forces in fibrous filters - a review. Powder Technol. 118, 166–170. https://doi.org/10.1016/S0032-5910(01)00307-2.

Sen Wang, C., Otani, Y., 2013. Removal of nanoparticles from gas streams by fibrous filters: a review. Ind. Eng. Chem. Res. 52, 5–17. https://doi.org/10.1021/ie300574m.

Subbiah, T., Bhat, G.S., Tock, R.W., Parameswaran, S., Ramkumar, S.S., 2005. Electrospinning of nanofibers. J. Appl. Polym. Sci. 96, 557–569. https://doi.org/10.1002/app.21481.

Trasande, L., Thurston, G.D., 2005. The role of air pollution in asthma and other pediatric morbidities. J. Allergy Clin. Immunol. 115, 689–699. https://doi.org/10.1016/j.jaci.2005.01.056.

Valavanidis, A., Fiotakis, K., Vlachogianni, T., 2008. Airborne particulate matter and human health: toxicological assessment and importance of size and composition of particles for oxidative damage and carcinogenic mechanisms. J. Environ. Sci. Heal. - Part C Environ. Carcinog. Ecotoxicol. Rev. 26, 339–362. https://doi.org/10.1080/10590500802494538.

Wang, Z.L., 2013. Triboelectric nanogenerators as new energy technology for self-powered systems and as active mechanical and chemical sensors. ACS Nano 7, 9533–9557. https://doi.org/10.1021/nn404614z.

WHO, 2013. Health effects of particulate matter. Policy implications for countries in eastern Europe, Caucasus and central Asia. WHO Reg. Off. Eur. 2013.

Wu, X., Wang, L., Yu, H., Huang, Y., 2005. Effect of solvent on morphology of electrospinning ethyl cellulose fibers. J. Appl. Polym. Sci. 97, 1292–1297. https://doi.org/10.1002/app.21818.

Xiao, J., Liang, J., Zhang, C., Tao, Y., Ling, G.-W., Yang, Q.-H., 2018. Advanced materials for capturing particulate matter: progress and perspectives. Small Methods 2, 1800012. https://doi.org/10.1002/smtd.201800012.

Yoon, H.J., Kim, D.H., Seung, W., Khan, U., Kim, T.Y., Kim, T., Kim, S.W., 2019. 3D-printed biomimetic-villus structure with maximized surface area for triboelectric nanogenerator and dust filter. Nanomater. Energy 63, 103857. https://doi.org/10.1016/j.nanoen.2019.103857.

Zhang, L., Liu, L., Pan, F., Wang, D., Pan, Z., 2012. Effects of heat treatment on the morphology and performance of PSU electrospun nanofibrous membrane. J. Eng. Fiber. Fabr. 7, 7–16. https://doi.org/10.1177/155892501200702s02.